

# Reconfigurable, multi-material, voxel-based soft robots

Julie Legrand,<sup>1\*</sup> Seppe Terryn,<sup>1</sup> Ellen Roels,<sup>1</sup>  
Bram Vanderborght<sup>1</sup>

<sup>1</sup> Robotics and Multibody Mechanics (R&MM) research group and Imec  
Vrije Universiteit Brussel, Brussels 1050, Belgium

\*To whom correspondence should be addressed; E-mail: julie.legrand@vub.be

**Voxel-based robots are aggregations of soft and simple building blocks that have been extensively evolved and simulated to perform various tasks, like walking, jumping or swimming. However, real-life voxel-based robots are rather scarce because of their challenging design and assembly. With the current materials and assembling methods, the interfaces between the soft multi-material voxels are prone to failure. This work proposes to make voxels out of reversible Diels-Alder polymers, which are available in a broad range of mechanical properties. By doing so, the covalent bonds at the multi-material interface ensure strong chemical connections, while allowing for reconfiguration. A first voxel-based gripper is thus robustly assembled, then disassembled, using its pieces (voxels) for reassembling another robot, i.e., a voxel-based walking robot. This reconfigurable property allows iterative validation of the simulated voxel-based robots and fine-tuning of the simulations parameters in a sustainable and economical way. Both physical voxel-based robots show similar behaviors as their simulations with root-mean-square errors down to 10.4%.**

## Introduction

Voxel-based soft robots (VSRs) are multi-material soft systems, formed by the aggregation of soft, simple building blocks called *voxels* (1). The word voxel originates from the word "pixel", where "vo" represents "volume". A voxel is therefore a representation of a three-dimensional space region which has its specific size, form and coordinate system. Voxels can either be active, e.g., they can be activated by volumetric actuation, or passive (2), and can be made of different materials varying from hard to soft. Thanks to their minimalist architecture, VSRs are intrinsically modular and reconfigurable, which makes that their design (body) and controller (brain) can easily be tailored for a specific task.

The interest of the robotic community for VSRs has grown during the last ten years (3) and originates from the limitations of soft robots. Soft materials are highly deformable, leading to inherent flexible, adaptable and safe systems. They can be stretched, compressed, bent, twisted and buckled and therefore offer an infinite number of degrees of freedom, which makes soft robotic system design and control very challenging (4). In order to deal with this complexity, researchers have used genetic algorithms to gradually built the soft robot and its control system based on the different interactions the robot experiences (2, 5–8). More specifically, the Compositional Pattern-Producing Network (CPPN), a type of Artificial Neural Networks (ANNs) which architecture evolution is guided by genetic algorithms (9), has been shown to be effective in creating lifelike, functional, complex objects (2, 10). Researchers have been using it to encode and evolve the body structure of soft robots resulting in 3D robots made of voxels (2, 6–8).

Although, VSRs have been extensively evolved and evaluated virtually (2, 6, 6, 7, 11–14), reports on physical VSRs are scarce (15–19). However, the authors believe that real-life experiments of evolved VSRs can not only help validate the optimized candidate, but also help tune complex model parameters (such as friction coefficients and damping ratios) to obtain efficient designs closer to reality. Iterative assessment of real-life optimized VSRs therefore needs to be conducted (20).

Khodambashi *et al.* (15, 21) built a VSR made of temperature-responsive hydrogel voxels. More specifically, the active voxels were made using poly(N-isopropylacrylamide) (PNIPAAm) based hydrogels which are electrically activated by Joule heaters. The hydrogel is placed with the Joule heater, i.e., a  $10\ \Omega$  resistor, in a cubic mold and is cured with a UV LED. When the resistor provides heat, the hydrogel volume decreases, while upon cooling, the hydrogel volume increases back. However, this actuation principle is limited to underwater condition and actuation speeds are limited (order of seconds). Kriegman *et al.* (16, 17) used pneumatic chambers as voxels, which allows more versatility in terms of applications and faster dynamics. The chambers are made from Dragon Skin 10 Fast (Smooth-On, Pennsylvania, USA)) and glued together using Sil-Poxy (Smooth-On, Pennsylvania, USA) in order to form the 3D voxel lattice.

In both above examples, the voxels are irreversibly glued together, preventing reconfiguration. Consequently, when used as an assessment tool to fine-tune the model parameters iteratively, each iteration has to be built from scratch, which represents a rather uneconomical and unecological approach. Moreover, these adhesives rely on secondary interactions, resulting in weak interfaces between the voxels, prone to damage after a limited number of actuation cycles. Vergara *et al.* (19) introduced reconfigurability in VSRs, by inserting magnets at each face of pneumatic voxels, allowing forming voxel lattices by magnetic attraction. However, the magnets prevent proper expansion of the voxel faces. Sui *et al.* (18) tackled this limitation by proposing to place the magnets on the edges of the voxels. Magnetically assembled VSRs can be easily reconfigured, however, the complexity of their design prevents their miniaturization, leading to bulky prototypes (18, 19).

On a more general note, as far as the authors are aware of, all the VSRs prototypes reported in the literature are made of one single material. This therefore limits their capabilities, preventing proper validation of the VSRs candidates and fine-tuning of the model parameters based on

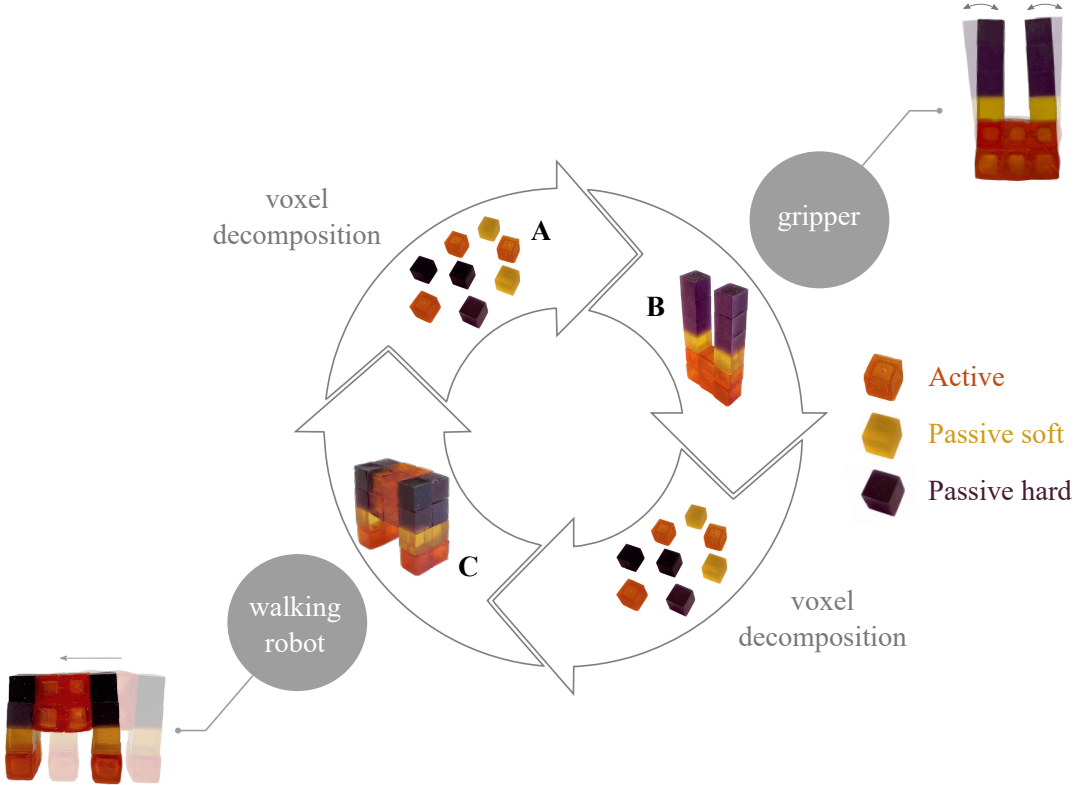


**Figure 1: Reconfiguration cycle of SH VSR.** (A) Individual active (red), passive soft (yellow) and passive hard (purple) voxels. (B) SH voxel-based soft gripper. (C) SH voxel-based soft walking robot.

real-life experiments.

The present work presents robust, multi-material, reconfigurable VSRs made of a self-healing (SH) polymer: the Diels-Alder (DA) polymer. The reversible covalent bonds of this polymer ensure high interfacial strength between the voxels while allowing for reconfiguration. Indeed, the reversible DA bonds allow recovering from macroscopic damage, like cuts and punctures, upon a heat-cool cycle (90°C) (22). Therefore, the polymer can be cut and healed back together to reform a single part with full recovery of the initial material properties (22). By varying the network properties of the polymer, different mechanical properties, ranging from hyperelastic (100 kPa) (23) to hard thermosets (10 GPa) (24) can be obtained leading to multi-material parts with strong multi-material interfaces (25).

This work takes advantage of the DA polymer characteristics to create robust, multi-material VSRs in a sustainable and economical way. Multiple passive and active voxels are manufactured from DA polymers with different mechanical properties (Fig.1). The voxels are assembled and bound together by heat stimuli, resulting in robust VSRs, with strong covalent bonds at the voxel interfaces. As the DA bonds are completely reversible, a VSR can thus be robustly assembled, then disassembled, using its pieces (voxels) for reassembling another robot (Fig.1). Since the assembly is material-based, the VSRs can be easily miniaturized. The lifetime of the built VSRs

can also be extended thanks to the SH capabilities of the material after damage. To demonstrate the feasibility of real-life, multi-material, reconfigurable VSRs, a SH voxel-based soft gripper was first made. Then the VSR was reconfigured into a self-healing voxel-based soft walking robot (Fig.1). The paper presents the detailed study on the development, manufacturing and reconfiguration DA-based VSRs, including the modelization and validation of single voxels and full VSRs.

## Results

### Multi-material voxel-based soft robot assembly

The voxels are made from three different DA polymers: a softer material (0.34MPa) for the active voxels, a middle-soft material (0.42MPa) for the passive soft voxels, and a harder material (0.92MPa) for the passive hard voxels (Figure 1). The material fabrication is described in the Materials and Methods section. The active voxels are pneumatic chambers, i.e., hollow inflatable cubes. They represent muscle cells in the VSR morphology (11). The voxels are 10×10×10mm large with a wall thickness of 2mm. The voxels are shaped using molds made of Ecoflex-00-30 (Smooth-On, Pennsylvania, USA). For the passive voxels, the mold consists in a cubic cavity with edges of 10mm. For the active voxels, one two-part mold is used to form 5 faces of the pneumatic chamber. The first part (Fig. 2A part 1) serves as a material container whereas the second part is put on top of the first part in order to form a cavity (Fig. 2A part 2). A second mold is used to make the last face of the active voxel, where a hole is foreseen for pneumatic connection (see Fig. 2A part 3). The DA polymers are poured in their respective molds and let for curing at 35°C for 48 hours. After curing and demolding (Fig. 2B), holes of about 2mm diameter are pierced in adjacent active voxels in order to create an air connection

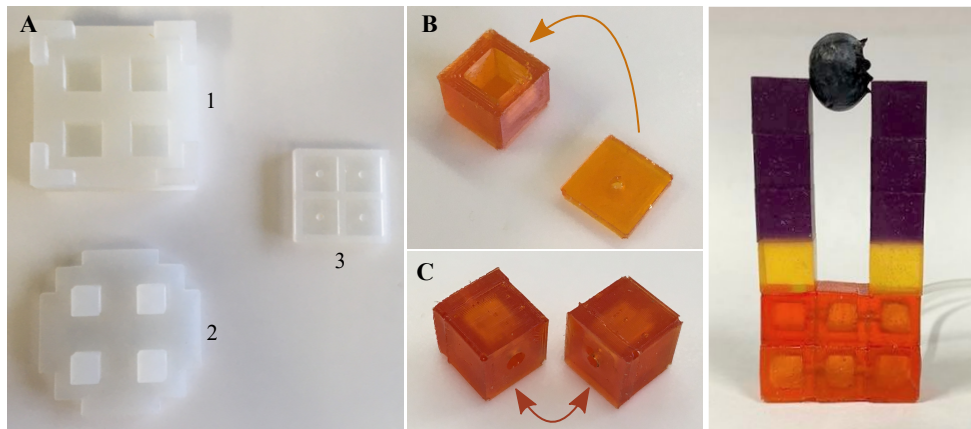


**Figure 2: Steps used to make the soft gripper.** (A) Molds used to make active voxels: 1. material receptor to form 5 faces of the pneumatic chamber; 2. top part of mold 1 to create the cavity of the pneumatic chamber; 3. mold for last face of the pneumatic chamber with hole foreseen for pneumatic connection. (B) Demolded open-pneumatic chamber and top face. (C) Assembling of two adjacent active voxels with fluid communication holes. (D) Assembled SH voxel-based soft gripper.

between them (Fig. 2C). This allows avoiding using a pneumatic connector for each active voxel. The last sixth face of the active voxel was then fixed to the open pneumatic chamber using uncured DA polymers in order to fill eventual gaps at the interface (Fig. 2B). After curing of the interface layer, the active voxel is warmed up at 90°C for 45 minutes to increase the mobility of the DA bounds and cooled down, let to heal, for 24 hours.

Using those voxels, a soft gripper was first built in order to demonstrate the feasibility of reconfigurable robust VSRs. The Supplementary Video S1 shows the complete manufacturing and assembling process of the soft gripper. The gripper is made out of 6 active voxels, 2 soft passive voxels and 6 hard passive voxels (see Figure 2D). To assemble the gripper, the active voxels were first fixed to each other using uncured DA polymers to ensure airtight interfaces, creating a block of active voxels. After curing of the interface, the passive voxels were put manually onto each other and on the active voxel block. The whole robot was placed in the oven at 90°C for 45 minutes to increase the mobility of the DA bounds and cooled down, let to heal, for 24 hours to obtain a voxel-based soft gripper made of different materials with robust interfaces. Finally, two pneumatic connections, i.e., two 2mm outer diameter, 1mm inner diameter silicon tubes were fixed to the active voxels using Sil-Poxy glue (Smooth-On, Pennsylvania, USA). Those silicone tubes were distally glued to a 4mm outer diameter polyethylene Festo air hose (Festo, Esslingen am Neckar, Germany) using a two-component Loctite 3430 epoxy glue (Loctite, Connecticut, USA) for easy plug of the tubing into the control valve.

## Voxel-based soft robot reconfiguration

The soft gripper is then reconfigured into a soft walking robot. The gripper voxels are therefore decoupled to obtain individual voxels and reuse them to make the walking robot (Fig. 1). To do so, two slicing guides, with notches of 0.35mm, were 3D printed with PLA (Fig. 3A). The first slicing guide is tailored to the gripper, while the second one is tailored to both upper and lower active voxel chambers. The gripper is first placed inside its tailored slicing guide, and the voxels are decoupled by manually slicing them using a 0.25mm thick Solingen blade (Solingen, Germany) in the notches of the guide (Fig. 3B). A similar operation is conducted for both active voxel chambers using the adapted slicing guide (Fig. 3C). The individual voxels are then taken out the slicing guide (Fig. 3D). To make the walking robot, eight additional active voxels, two soft passive voxels and two hard passive voxels are needed. Both active voxels with fixed pneumatic connection from the gripper are not needed anymore because the placement of the communication hole in those voxels do not match the design of the walking robot active voxels. The active voxels are fixed to each other using uncured DA polymers to ensure airtight interfaces, creating blocks of active voxels (Fig. 3E). After curing of the interface, the passive voxels are put manually onto each other and on the active voxel block. The walking robot is then placed in the oven at 90°C for 45 minutes and cooled down, let to heal, for 24 hours to obtain a reconfigured voxel-based walking robot made of different materials with robust interfaces (Fig. 3F). Finally, four pneumatic connections similar to the ones used for the soft gripper are glued to the four active voxel chambers of the walking robot.

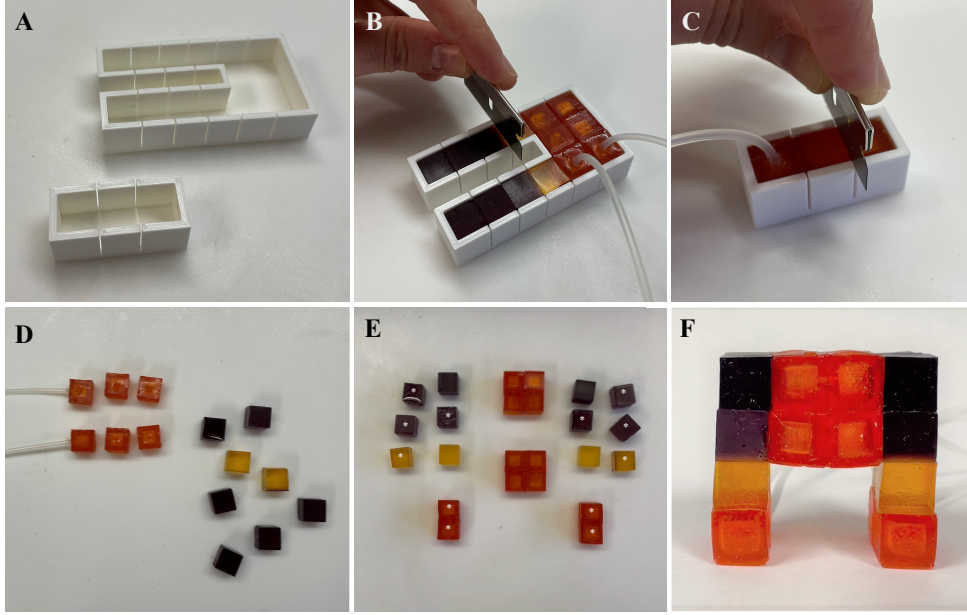


**Figure 3: Reconfiguration steps used to make the walking robot.** (A) Slicing guide tailored to the gripper (top) and to the upper and lower active voxel chambers (bottom). (B) Slicing of the gripper using a sharp blade. (C) Slicing of the active voxel chamber using a sharp blade. (D) Sliced voxels of the gripper. (E) Addition of 8 active voxels, 2 soft passive voxels and 2 hard passive voxels to the gripper's voxels (marked with a white star) for the assembly of the walking robot. (F) Assembled SH voxel-based walking robot.

## Active voxels characterization

The active voxels are inflated using a sinusoidal input pressure signal, which is the conventionally used Central Pattern Generator (CPG) of VSRs (7, 8, 11, 17). Note that, in contrast to simulated active voxels, which expand and contract, only expansion of the voxel was physically performed. The compression of a pneumatic chamber causes buckle and therefore was discarded (17).

The pneumatic active voxels are characterized by studying the inflation of four different voxels using a sinusoidal input pressure signal of amplitude 0.45bars. This is the maximum amplitude an active voxel could withstand. Above this amplitude, the silicone pneumatic connection, which is fixed to the SH material using a silicone glue, comes off from the voxel. The section surface of each active voxel with respect to the section surface at rest is calculated under pressurization using an image segmentation algorithm described in the Materials and Methods Section. The mean and standard deviation (SD) of those tests are reported in Fig. 4. The section surface of the active voxel can expand up to a maximum of  $7.6\text{mm}^2$  as compared to its rest state. The active voxel was also simulated in VoxCAD, a software package allowing the simulation of soft materials under large deformations (26), and compared to the experiments (see Fig. 4 A and B). VoxCAD is the most commonly used VSR simulator. The maximum contraction of the simulated voxel was considered as the rest state such that it could be compared to the only expanding physical voxel. A Root-Mean-Square Error (RMSE) of 12.3% was calculated

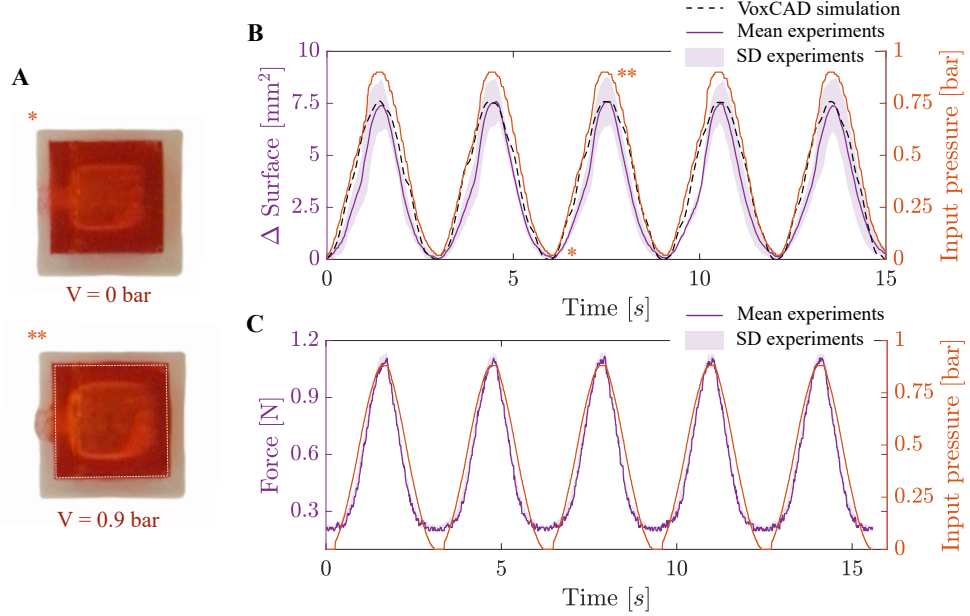


**Figure 4: Active voxels characteristics.** (A) Picture of an active voxel on a support under 0 and 0.9 bar (indices \* and \*\* refer to subfigure B). The dotted line represents the voxel outline at rest, under 0 bar. (B) Section surface of an active voxel. (C) Active voxel generated force. The mean and SD of the experimental data is calculated from the measurements taken on 4 different active voxels.

between the simulations and the experiments. The mean and SD of the force generated by an active voxel was also measured by performing the tests on four different voxels. An active voxel can generate a maximum force of 1.12N in average (Fig. 4C).

## Soft gripper

The gripper is composed of two chambers (upper and lower) containing each three connected active voxels, two passive soft voxels and six passive hard voxels (see Fig. 1B). Each voxel is  $10 \times 10 \times 10\text{mm}$  large. The gripper was tested and characterized. To do so, the active voxel chambers of the gripper were actuated asynchronously and synchronously using sinusoidal inputs pressure signals of different frequencies and of amplitude 0.3bars. Above this amplitude, the pneumatic connections come off from the voxels. Asynchronous actuation makes the gripper open and close like a pendulum whereas synchronous actuation makes the gripper opening larger while maintaining the fingers parallel to each other (Fig. 5A).

The position of each finger extremity was calculated by tracking markers using a camera. This tracking method is described in details in the Materials and Methods Section. As a result, the distance between both finger extremities could be measured under asynchronous and synchronous actuation (Fig. 5B). At rest, the distance between both fingers is 20mm. The distance reaches a maximum of 22.67mm and a minimum of 17.49mm when the gripper is actuated asynchronously, and a maximum of 20.56mm when actuated synchronously.

To test the dynamic behavior of the gripper, it was actuated under three different input signal frequencies (i.e. 0.4, 0.6 and 0.9 Hz) (Fig. 5BC). As the frequency increases, the maximum and minimum distance between the gripper's fingers decreases. This is due to the dynamic behavior of the soft materials (27). Under similar stresses, high-speed deformation will lead to smaller deformations than when deformed at lower speed.

The force generated by the gripper when actuated asynchronously was also measured at different frequencies. To do so, a load cell was placed against the inner surface of the left finger. During this test, the left finger was therefore blocked, immobile against the load cell. As visible in Fig. 5E and F, the generated force is small (smaller than 0.02N) and is not affected by an increase of the input signal frequency. The fact that the force is relatively small is due to the small size of the active voxel chambers and the low stiffness of the gripper's base (0.42 MPa).

The soft gripper was also simulated in VoxCAD and compared to the experiments (Fig. 5A and D). When actuated asynchronously, the RMSE between the simulated and experimental finger's position are 0.32mm (10.41%) and 0.53mm (15%) for the horizontal displacement (along the x-axis in Fig. 5A) of the left and right finger, respectively. This result shows that the simulations can represent the real horizontal movement of the gripper's finger with a rather good accuracy (Fig. 5D). However, the RMSE is larger for the vertical finger's position (along the y-axis in Fig. 5A): 0.45mm and 0.68 for the left and right finger, respectively. The simulated vertical finger's position stays more or less constant during actuation, whereas the experimental one increase and decreases depending on the actuated chamber. This is due to manufacturing inaccuracies causing the upper chamber to inflate slightly more than the lower one causing a gripper's vertical displacement of 0.4mm.

When actuated synchronously, the simulated and experimental displacement of the gripper's fingers show similar behavior (Fig. 5D). For the horizontal displacement, the movement amplitudes of the simulated and physical gripper's fingers are very similar: a slightly larger amplitude (0.56mm) for the experimental left finger position than the simulated one (0.44mm) and the exact same amplitude of 0.46mm for the right finger position. When looking at the vertical displacement, the amplitude is slightly larger for the experimental left (0.8mm) and right (0.8mm) finger position than the simulated ones (0.7mm and 0.73mm respectively). However, an offset is present between the simulated and experimental displacement values (Fig. 5D). This is due to the fact that simulated voxels can expand and contract, whereas the physical ones can only expand. If the voxel contraction of a chamber could be compensated by the expansion of the other chamber during asynchronous actuation, this is not the case during synchronous actuation. Therefore, the simulated finger tip positions will decrease below the rest position during contraction, whereas the experimental finger tip positions will stay above it.

Thanks to the SH property of DA polymers, the lifetime of the VSRs can also be extended. To illustrate this, the gripper was damaged by creating a small cut in the middle active voxel of the bottom chamber (Supplementary Fig. S1A and B). After damage, the gripper could not close properly anymore. The distance between the damaged gripper's fingers could only reach a minimum of 18.8mm. Also, the gripper took more time to close since the lower chamber, which

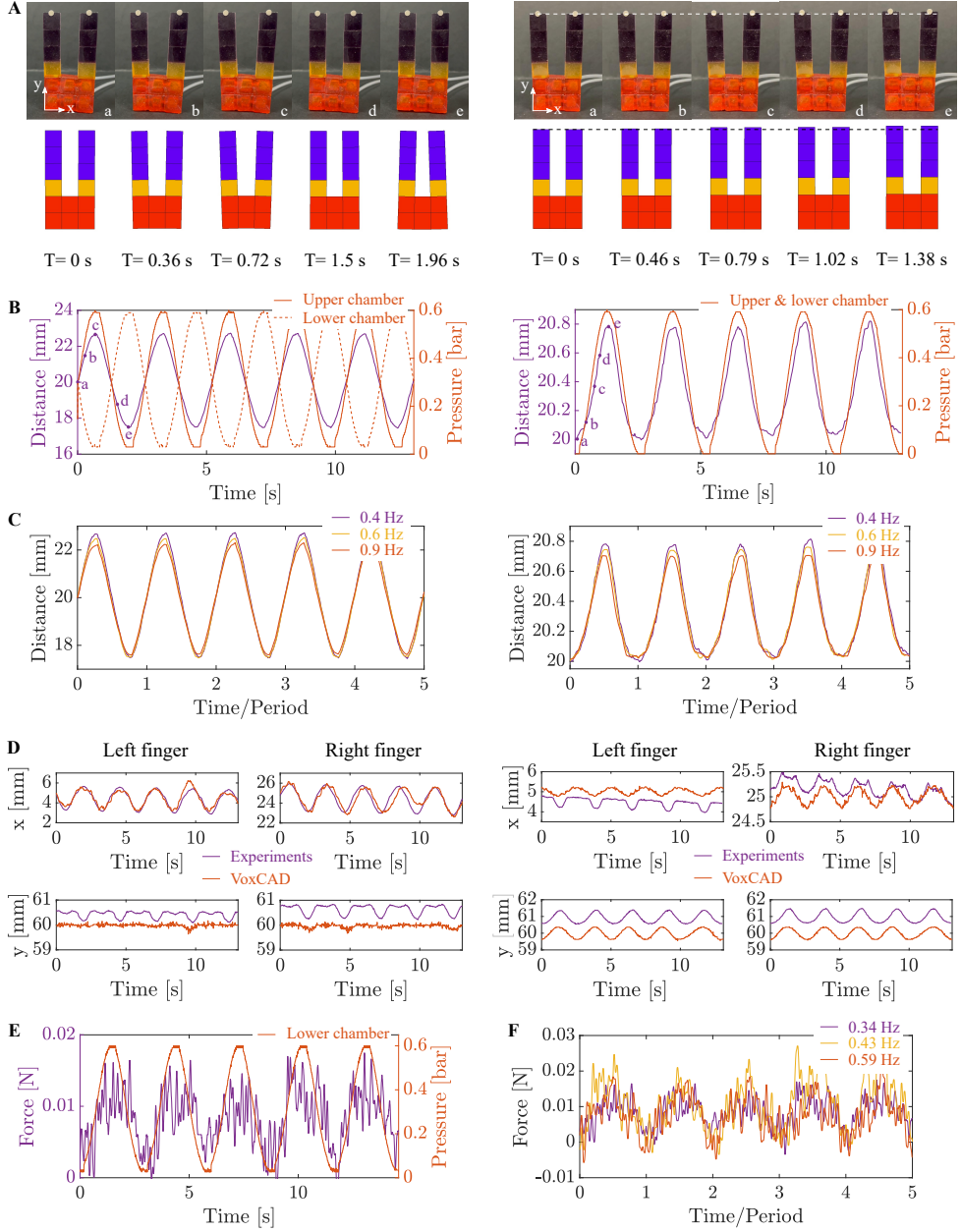


**Figure 5: SH voxel-based soft gripper characterization.** (A) Experimental (top) and simulation (bottom) pictures of the gripper under asynchronous (left) and synchronous (right) actuation at different times  $T$  in the actuation cycles. The letters correspond to the points in (B). (B) Distance between the gripper fingers and corresponding pressure under asynchronous (left) and synchronous (right) actuation. (C) Distance between the gripper fingers at different actuation frequencies under asynchronous (left) and synchronous (right) actuation. (D) Experimental and simulated positions of the left and right fingers under asynchronous (left) and synchronous (right) actuation. (E) Gripper force and corresponding pressure. (F) Gripper force at different actuation frequencies.

makes the gripper close, could not inflate properly anymore. The gripper was healed according to the protocol described in the Materials and Methods Section. After healing, the gripper could retrieve its full opening and closing capability, even at high frequencies (Supplementary Fig. S1C).

## Soft walking robot

The voxel-based soft gripper was reconfigured into a voxel-based soft walking robot. Twelve of the 14 voxels composing the gripper were reused to make the walking robot. Eight active voxels, 2 soft passive voxels and 2 hard passive voxels were added as well. The walking robot is composed of four chambers, one at each foot of the robot composed of 2 active voxels, and two larger chambers, each composed of 4 active voxels, placed one upon another creating the core of the walking robot (Fig. 6A). To make the robot walk, the upper core chamber and the left foot chamber were actuated together (marked as "+" in Fig. 6A) asynchronously with respect to the lower core and the right foot chambers (marked as "-" in Fig. 6A) using sinusoidal inputs pressure signals of different frequencies and of amplitude 0.3bars. When actuated at a frequency of 0.4Hz, the robot could travel 16.9mm in 53s (Fig. 6A and D). This distance was calculated by tracking the marker placed on the right leg with a camera using the tracking method described in the Materials and Methods Section. During its course, the robot's maximum velocity was 2.9mm/s (Fig. 6D). Increasing the actuation frequency does not necessarily make the robot proportionally walk faster (Fig. 6C). At a frequency of 0.4 and 0.9Hz, the robot traveled 10mm after 10 actuation cycles. However, At a frequency of 0.6Hz, the robot only traveled 8.5mm after 10 actuation cycles. This phenomenon is due to the variable friction between the robot's feet and the ground. The roughness of the robot's feet is not even on the entire foot due to the molding process of the material. Moreover, the roughness can also change according to the input pressure, since inflation of the robot's foot cause its surface to stretch.

The soft walking robot was also simulated in VoxCAD and compared to the experiments (Fig. 5B and E). In 26.5s, the simulated walking robot could only travel 4.4mm, whereas the experimental could travel 9.7mm. This is due to the friction coefficient value and the Ground Damp Ratio (GDR) chosen for the simulations. The parameters for the static and dynamic friction coefficients, i.e., 1 and 0.5 respectively, were adopted from Kriegman *et al.* (17) who used silicone (Dragon Skin 10 Fast, Smooth-On, Pennsylvania, USA) for the making of their voxels. Those parameters do probably not exactly reflect the real friction between the robot's foot and the ground, but obtaining a value for this coefficient is challenging. Indeed, the roughness of the robot foot is not even due to the molding process of the material using 3D printed molds and the friction coefficient changes in function of the inflation pressure in the robot's foot. Therefore, the study of friction at the feet of the robot is beyond the scope of this paper and the estimations used by Kriegman *et al.* (17) were chosen for the simulations. The GDR, however, can be tuned. Whereas a value of 0.1 was first chosen, the error between the simulations and the experiments could be reduced by fixing the GDR to 0.05. With this value, the simulated walking robot could travel 11.6mm in 26.5s.

The self-healing properties of the used material were again tested. To do so, the walking robot was first damaged at its upper core chamber. This resulted in a shorter traveled distance for all

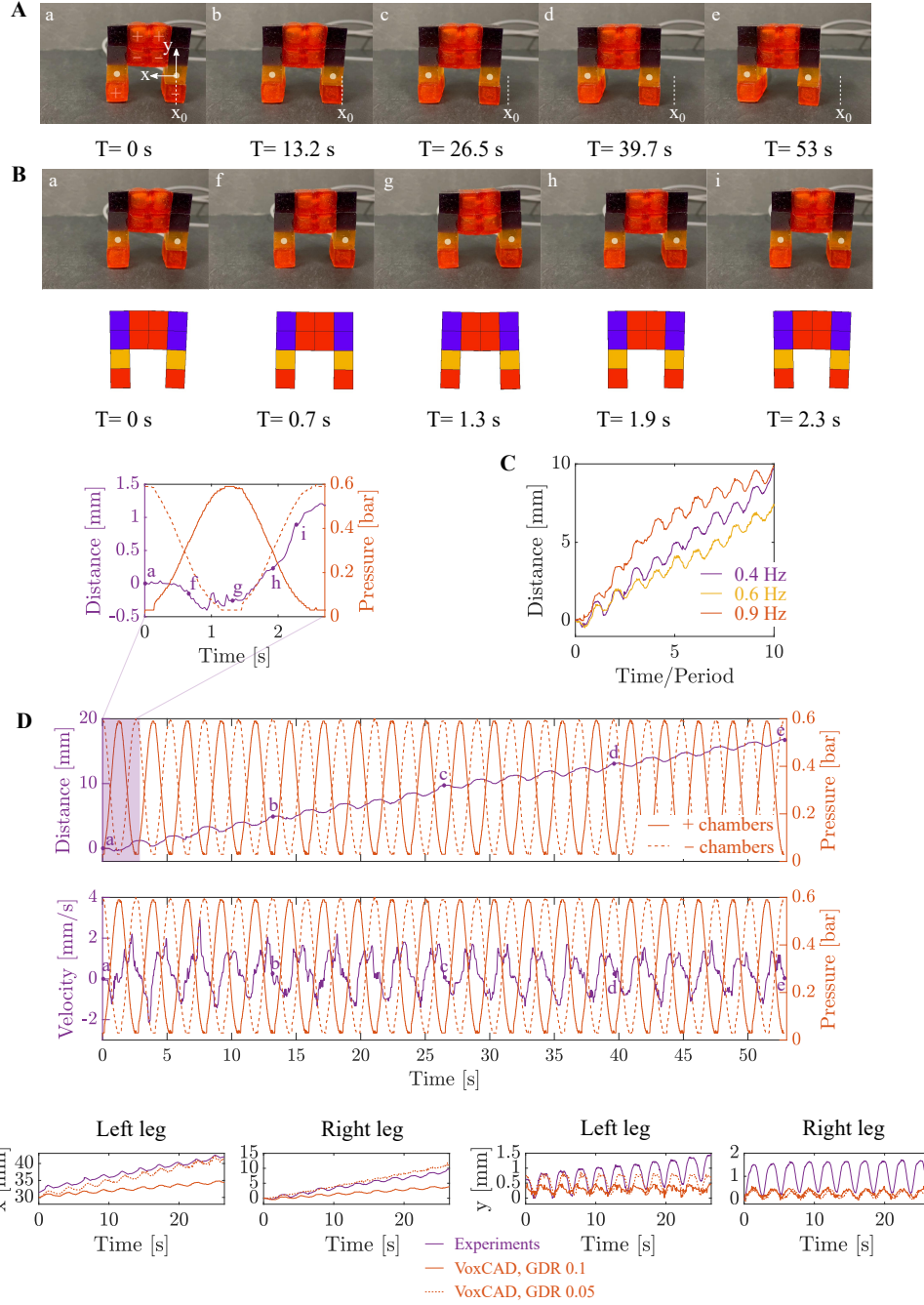


**Figure 6: SH voxel-based soft walking robot characterization.** (A) Experimental pictures of the walking robot under asynchronous actuation of its chambers during 53s. The letters correspond to the points in (D). (B) Experimental (top) and simulation (bottom) pictures of the walking robot under asynchronous actuation of its chambers during one actuation period. (C) Distance traveled by the right leg of the robot at different actuation frequencies. (D) Distance traveled by the right leg (top) and velocity of the robot (bottom) in function of the input pressure. (E) Experimental and simulated (with two different Ground Damp Ratios) positions of the left and right legs of the robot.

frequencies tested (Supplementary Fig. S2C). After healing, the robot could retrieve its initial ability to walk at a faster pace. Actually, healing the robot made it walk even faster when actuated at 0.4 and 0.6Hz. This is due to a change in the polymer microstructure after thermal treatment. The polymer becomes softer and "stickier" and the friction coefficient between the polymer and the ground increases. However, those changes tend to stabilize with time (28).

## Multi-material interface robustness

VRSs intrinsically consist of multiple interfaces, i.e., maximum six interfaces per voxel. Therefore, robust yet reconfigurable interfaces between the voxels are essential for the proper actuation and reconfigurability of VSRs. To do so, SH materials and more specifically DA polymers were chosen to make the voxels. DA polymers are networks containing reversible covalent crosslinks (29). This means that isothermal heat treatment followed by a controlled cooling allows reforming the covalent crosslinks inside the materials and at the interface of two different DA polymers, i.e. with two different mechanical properties (25), after a cut inside the material or at the multi-material interface. To demonstrate the feasibility of robust reconfigurable VSRs, three different materials were chosen to make the demonstrators, a softer material (0.34 MPa) BMI-1400-FT5000-r0.7 (orange material in Fig. 7), a middle-soft material (0.42 MPa) BMI-689-FT5000-r1 (yellow material in Fig. 7) and a harder material (0.92 MPa) BMI-689-FT3000-r0.6 (purple material in Fig. 7). More information on the material characterization is available in the Materials and Methods Section. In order to demonstrate the reconfigurability of multi-material voxels, three batches of each three different material combinations were tested. The first batch contains multi-material samples that were healed only once (Fig. 7B) according to the healing method described in the Materials and Methods Section. The second batch contains samples that were healed and cut at the multi-material interface (see Fig. 7A) three times consecutively using a 0.25mm thick Solingen blade (Solingen, Germany) (Fig. 7C). The third batch represents samples that were healed and cut at the multi-material interface five times consecutively (Fig. 7D). All samples were then, after the healing and cutting cycles, stretched using a uniaxial tensile machine and the fracture locations were analyzed. As visible in Fig. 7, the fracture is not located at the multi-material interface for any of the samples, however, it is located in the weakest material (Table 1). This shows that even after cutting and healing the multi-material interface five times, the interface is still robust. The VSRs can thus be reconfigured multiple times (at least 5 times) using its same pieces (voxels).

Table 1: Fracture stresses of multi-material samples

Sample	1 H-C cycle	3 H-C cycles	5 H-C cycles	Weakest material max. stress
soft - middle soft	0.12 MPa	0.11 MPa	0.11 MPa	middle - soft: 0.14 MPa
soft - hard	0.18 MPa	0.17 MPa	0.19 MPa	hard: 0.17 MPa
middle soft - hard	0.15 MPa	0.15 MPa	0.12 MPa	middle - soft: 0.14 MPa

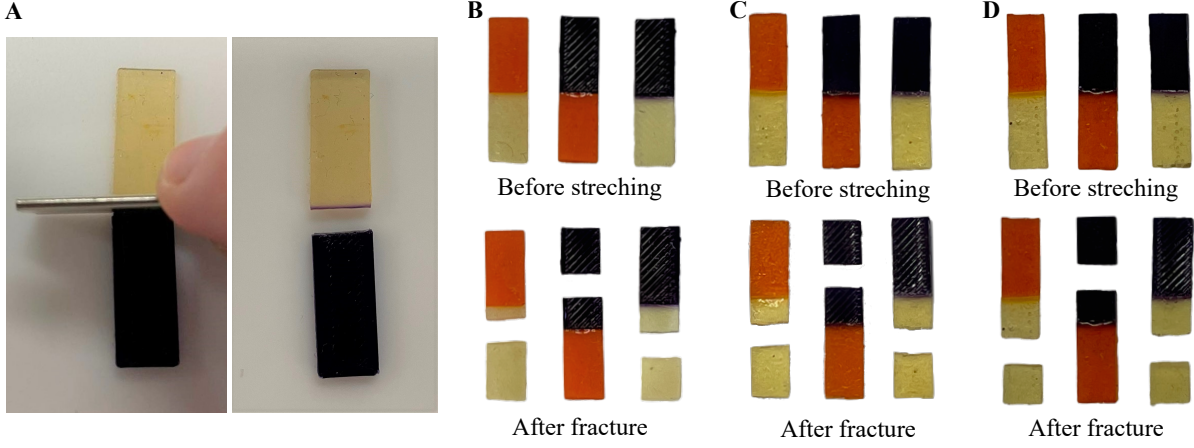


**Figure 7: Test of the robustness and reconfigurability of the multi-material interface.** Orange material: softer material (0.34 MPa) BMI-1400-FT5000-r0.7. Yellow material: middle-soft material (0.42 MPa) BMI-689-FT5000-r1. Purple material: harder material (0.92 MPa) BMI-689-FT3000-r0.6. (A) Cut at the material interface using a sharp blade. (B) Multi-material samples healed once together. (C) Multi-material samples after three healing and cutting cycles. (D) Multi-material samples after five healing and cutting cycles.

## Discussion

The physical assembly of VSRs can help closing the simulation-to-reality-gap (30) by making the experimental validation of the virtually evolved VSRs candidates possible and allowing tuning the model parameters, such as friction coefficients and damping ratios. Those processes are often iterative and therefore require a reconfigurable experimental platform. This work therefore describes for the first time the making and reconfiguration of VSRs made of DA polymers. The reconfiguration is based on the intrinsic material properties of the voxels. Consequently, this approach is easily scalable and VSRs can be miniaturized. Reconfiguration was demonstrated by building a voxel-based walking robot out of a voxel-based gripper. Both robots were tested and the results were compared to the most commonly used VSR simulator: VoxCAD. Especially for the walking robot, which directly interacts with the environment, the proper VoxCAD parameter choice was crucial to obtain similar walking behavior in simulations and in reality. Dividing the ground damp ratio by two resulted in a doubling of the simulated robot speed, which was closer to the experimental robot speed. This shows that proper tuning of the simulator parameters is essential to create efficient VSRs that will also behave efficiently in reality.

If reconfiguration of the physical VSRs is important to avoid building numerous prototypes from scratch, the robustness of the reconfigured VSRs is equally crucial. The loosening of some VSRs voxels could affect the experimental results. This is why DA polymers were used in this work to make the voxels. The reversible covalent bonds of this polymer ensure high interfacial strength between the voxels while allowing for reconfiguration. The interfacial strength of reconfigured interfaces was tested by repeatedly (up to 5 times) cutting and healing multi-material interfaces. Even after 5 reconfiguration cycle, the multi-material interface was still

stronger than the weakest material of the sample. This robustness is further increased by the healing capacity, intrinsic to the VSRs material: the DA polymers.

The presented reconfigurable VSR design and assembly method can be used to perform future research on evolved VSRs while reducing material costs, manufacture labor and waste production. Aside from research on evolutionary VSRs, the presented reconfigurable approach can have a beneficial impact on the manufacturing, reconfiguration and recycling of future soft robots. The approach would therefore address the current sustainability issues of the traditional elastomeric materials that are broadly used today.

## Materials and Methods

### Material fabrication

The voxels are made out of DA polymers, which are networks containing reversible covalent crosslinks formed by a DA bond between a furan and a maleimide. The particularity of those polymers is that they can heal (i.e. reforming covalent crosslinks) after damage by applying an isothermal heat treatment under their gel temperature. More specifically, heating the damaged material allows for an increase of mobility of the DA bounds. When cooling the material, the DA bounds can reform which recreates a strong interface at the damage region (22). For the active voxels, the bismaleimide BMI-1400 was used together with the furan-functionalized Jeffamine FT5000 with a ratio maleimide/furan of 0.7. FT5000 was obtained by irreversibly binding furfuryl glycidyl ether (FGE) on a Jeffamine JT5000 using an epoxy-amine reaction. For the soft passive voxels, the bismaleimide BMI-689 was used together with FT5000 with ratio with a ratio maleimide/furan of 1. For the hard passive voxels, the bismaleimide BMI-689 was used together with FT3000 in a maleimide/furan-ratio of 0.6. Like FT5000, FT3000 is obtained through an epoxy-amine reaction between Jeffamine JT3000 and FGE. Those particular materials were chosen because of their low Young modulus and their similar gel temperature (see Table 2). Indeed, in order to proceed to the healing, the material first need to be warmed up at a high temperature below the gel temperature, it is important that both material have a similar gel temperature. This can ensure proper mobility in both materials during the isothermal phase, and therefore proper healing without loosing mechanical stability, e.g., plastic deformation or flow, when heating the materials above their gel temperatures. The gel temperatures of the different material were determined by dynamic rheology experiments using the Discovery Hybrid Rheometer-3 of T.A. Instruments (Waters Corporation, Massachusetts, USA). To do so, the evolution of the material's storage and loss modulus were evaluated during a temperature ramp and at multiple frequencies (from 0.3 to 3.1 Hz). In Fig. 8A,  $\delta$  represents the phase angle between the stimulus (stress) and the response (strain). In dynamic rheometry the gel temperature is best defined as the temperature at which  $\delta$  is frequency independent (31), i.e., at the intersection of the iso-frequency lines (see Fig. 8A). In order to determine the Young's modulus of the different materials, 3 tensile tests were realized per material (Fig. 8B) using the Q800 Dynamic Mechanical Analyzer of T.A. Instruments (Waters Corporation, Massachusetts, USA). The Young's moduli reported in Table 2 were calculated at 2% deformation.

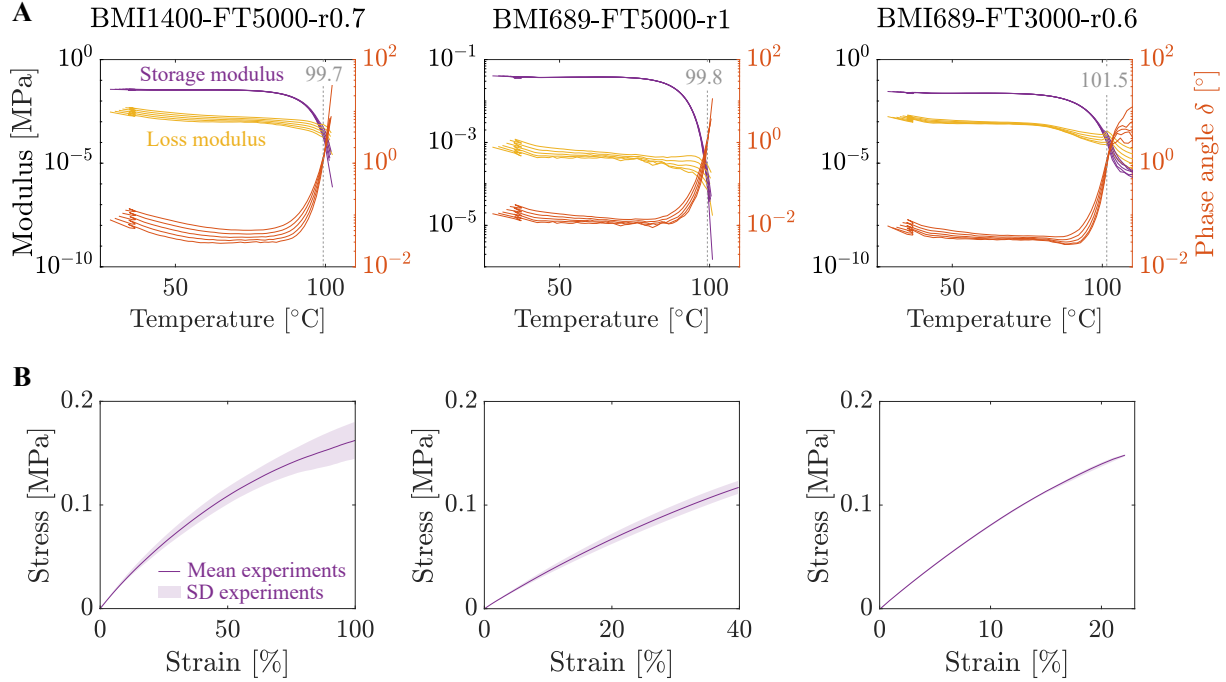


**Figure 8: SH material characterization.** (A) Rheological experiments for the determination of the gel temperature of the different materials used in the SH VSRs. The different curves represent different frequencies (from 0.3 to 3.1 Hz) (B) Stress-strain curves of the different materials used in the SH VSRs. The mean is taken on 3 measurement curves.

Table 2: Voxel material properties

Material	Modulus [MPa]	Max. stress [MPa]	T <sub>gel</sub> [°C]
BMI-1400-FT5000-r0.7	0.34	0.19	99.7
BMI-689-FT5000-r1	0.42	0.14	99.8
BMI-689-FT3000-r0.6	0.92	0.17	101.5

## Characterization

In order to characterize the active voxels and both voxel-based soft robots, different set-ups and algorithms were used. Actuating the active voxel and measuring the generated force was done using dedicated set-ups whereas the measurement of the voxel expansion and the robot's movements was realized using specific algorithms.

### Input pressure set-up

The input pressure was set using a pressure regulator valve VEAB-L-26-D7-Q4-V1-1R1 (Festo, Esslingen am Neckar, Germany). To control the regulator valve, an Arduino is used with a PWM signal and a low-pass filter.

## **Force measurement set-up**

To measure the force generated by a single active voxel and the voxel-based gripper, a miniature S-beam load cell from Futek (Irvine, USA) was used. For the single voxel tests, the load cell was attached to a fixed column. The voxel was placed under the load cell, nearly touching it. Under pressurization, the voxel would expand and push on the load cell, allowing recording the generated force using an Arduino. For the voxel-based gripper, the load cell was placed against the inner surface of the left finger.

## **Image segmentation algorithm**

In order to measure the active voxel expansion, an image segmentation algorithm was used. Its purpose is to measure the section area of an active voxel under pressurization. To do so, a Matlab (Mathworks, California, USA) program was written to segment the orange color of the active voxel and provide a black and white image, with the active voxel in white for each frame of the recorded video. Then, the Matlab function *bwarea()* calculates the number of white pixels from the binary image. The number of pixels was scaled in order to obtain the section area. The segmentation process is illustrated in Supplementary Fig. S3A. Note that the voxel was placed on a hollow support (visible in Supplementary Fig. S3A) to avoid the face making contact with the table to raise the voxel under pressurization, making the section area larger.

## **Marker tracking algorithm**

To track markers placed on the voxel-based soft robot, a self-written algorithm using the Matlab function *imfindcircles()* was used on each frame of the recorded video. This tracking algorithm can predict a marker position with a 0.09 mm accuracy (32). An illustration of the marker tracking is given in Supplementary Fig. S1B.

## **Voxel-based robot modelization**

To simulate the behavior of both the VSRs, i.e., the gripper and the walking robot, VoxCAD, a software that can simulate soft materials under large deformations was used. Table 3 and 4 gathers the parameters that were used for the simulation of both VSRs. In VoxCAD, the amplitude of the input sinusoidal signal is regulated by changing the temperature of the environment. The maximum value of the temperature for the single active voxel simulation was chosen in Table 4 by finding which temperature leads to the same maximum deformation of an experimental active voxel (Fig. 4). For the gripper and walking robot simulations, the maximum value of the temperature in Table 4 was chosen by picking the corresponding temperature value to the deformation of an experimental active voxel at 0.6bars (maximum input pressure used for the gripper and walking robot tests).

Table 3: VoxCAD parameters: voxels

Parameter	Active voxel	Soft passive voxel	Hard passive voxel
Voxel Dim (mm)	10	10	10
Material type	basic	basic	basic
Elastic modulus (MPa)	0.34	0.42	0.92
Material model	linear	linear	linear
Poissons Ratio	0.44	0.44	0.44
Density (Kg/m <sup>3</sup> )	852	972	989
CTE (1/°C)	0.01	0	0
Temp Phase (rad)	0	0	0
Static Fric Coeff	1	1	1
Dynamic Fric Coeff	0.5	0.5	0.5

Table 4: VoxCAD parameters: VSRs simulation

Parameter	Single active voxel	Soft gripper	Soft walking robot
Timestep (% optimal dt)	0.166	0.166	0.166
Ground damp ratio	0.1	0.1	0.1, 0.5
Temperature (°C)	36	27	27
Period (sec)	3	2.4	2.4
Gravity (m/s <sup>2</sup> )	9.81	9.81	9.81

## References

1. J. Bhatia, H. Jackson, Y. Tian, J. Xu, W. Matusik, *Advances in Neural Information Processing Systems* **34** (2021).
2. N. Cheney, R. MacCurdy, J. Clune, H. Lipson, *ACM SIGEVolution* **7**, 11 (2014).
3. J. Hiller, H. Lipson, *IEEE Transactions on Robotics* **28**, 457 (2011).
4. D. Rus, M. T. Tolley, *Nature* **521**, 467 (2015).
5. J. Rieffel, *et al.*, *Proceedings of the 11th annual conference companion on genetic and evolutionary computation conference: Late breaking papers* (2009), pp. 2499–2504.
6. N. Cheney, J. Bongard, H. Lipson, *Proceedings of the 2015 annual conference on Genetic and Evolutionary Computation* (2015), pp. 935–942.
7. T. Kimura, Z. Jin, R. Niiyama, Y. Kuniyoshi, *2016 IEEE/SICE International Symposium on System Integration (SII)* (IEEE, 2016), pp. 409–414.
8. N. Cheney, J. Clune, H. Lipson, *ALIFE 14: The Fourteenth International Conference on the Synthesis and Simulation of Living Systems* (MIT Press, 2014), pp. 222–229.

9. K. Ghaderi, F. Akhlghian, P. Moradi, *2012 2nd International eConference on Computer and Knowledge Engineering (ICCKE)* (IEEE, 2012), pp. 12–17.
10. J. Clune, H. Lipson, *ACM SIGEVolution* **5**, 2 (2011).
11. N. Cheney, J. Bongard, V. SunSpiral, H. Lipson, *Journal of The Royal Society Interface* **15**, 20170937 (2018).
12. D. Gravina, A. Liapis, G. N. Yannakakis, *Proceedings of the Genetic and Evolutionary Computation Conference Companion* (2017), pp. 61–62.
13. K. Walker, H. Hauser, *ALIFE 2021: The 2021 Conference on Artificial Life* (MIT Press, 2021).
14. T. Kimura, R. Niiyama, Y. Kuniyoshi, *2021 IEEE 4th International Conference on Soft Robotics (RoboSoft)* (IEEE, 2021), pp. 295–301.
15. R. Khodambashi, S. Berman, X. He, D. M. Aukes, *2021 IEEE 4th International Conference on Soft Robotics (RoboSoft)* (IEEE, 2021), pp. 571–574.
16. S. Kriegman, *et al.*, *arXiv preprint arXiv:1905.09264* (2019).
17. S. Kriegman, *et al.*, *2020 3rd IEEE International Conference on Soft Robotics (RoboSoft)* (IEEE, 2020), pp. 359–366.
18. X. Sui, *et al.*, *Applied Sciences* **10**, 294 (2020).
19. A. Vergara, Y.-s. Lau, R.-F. Mendoza-Garcia, J. C. Zagal, *PloS one* **12**, e0169179 (2017).
20. G. Shao, A. Brodsky, P. Ammann, C. McLean, *Proceedings of the industrial simulation conference 2009* (2009), pp. 323–327.
21. R. Khodambashi, *et al.*, *Advanced Materials* **33**, 2005906 (2021).
22. S. Terryn, J. Brancart, D. Lefeber, G. Van Assche, B. Vanderborght, *Science Robotics* **2** (2017).
23. S. Terryn, J. Brancart, E. Roels, G. Van Assche, B. Vanderborght, *IEEE Robotics & Automation Magazine* **27**, 44 (2020).
24. S. Terryn, *et al.*, *Bioinspiration & biomimetics* **10**, 046007 (2015).
25. S. Terryn, E. Roels, J. Brancart, G. Van Assche, B. Vanderborght, *Actuators* (Multidisciplinary Digital Publishing Institute, 2020), vol. 9, p. 34.
26. J. Hiller, H. Lipson, *Soft robotics* **1**, 88 (2014).
27. W. W. Chen, B. Song, *Dynamic Failure of Materials and Structures* (Springer, 2009), pp. 1–28.
28. A. Safaei, S. Terryn, B. Vanderborght, G. Van Assche, J. Brancart, *Polymers* **13**, 2522 (2021).

29. S. Terryn, *et al.*, *Materials Today* (2021).
30. S. Doncieux, N. Bredeche, J.-B. Mouret, A. E. G. Eiben, *Frontiers in Robotics and AI* **2**, 4 (2015).
31. H. H. Winter, *Polymer Engineering & Science* **27**, 1698 (1987).
32. J. Legrand, *et al.*, *IEEE robotics and automation letters* **3**, 4359 (2018).

## Acknowledgments

This work has received funding from the SHERO project, a Future and Emerging Technologies (FET) program of the European Commission (grant agreement ID 828818), as well as the personal FWO grants of Legrand (12Y8622N), Terryn (FWOTM784) and Roels (1S84120N).

## Supplementary materials

Figs. S1 to S3

Video S1

## Supplementary figure

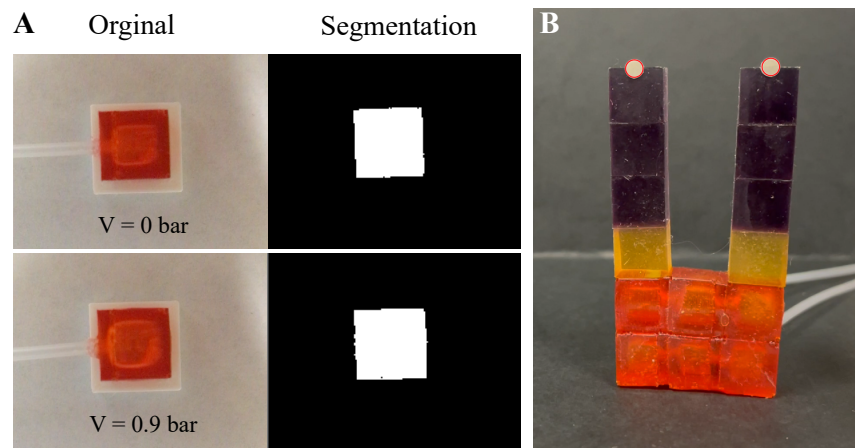


Figure 1: **Image treatment algorithms for the characterization of active voxels and voxel-based soft robots.** (A) Segmentation of an active voxel to calculate its section area. (B) Tracking of markers (marked in red) placed on a voxel-based soft robot for its characterization.